LETTER

doi:10.1038/nature17635

A high-temperature ferromagnetic topological insulating phase by proximity coupling

Ferhat Katmis[1,2,3]*, Valeria Lauter[4]*, Flavio S. Nogueira[5,6], Badih A. Assaf[7,8], Michelle E. Jamer[7], Peng Wei[1,2,3], Biswarup Satpati[9], John W. Freeland[10], Ilya Eremin[5], Don Heiman[7], Pablo Jarillo-Herrero[1] & Jagadeesh S. Moodera[1,2,3]

Topological insulators are insulating materials that display conducting surface states protected by time-reversal symmetry[1,2], wherein electron spins are locked to their momentum. This unique property opens up new opportunities for creating next-generation electronic, spintronic and quantum computation devices[3–5]. Introducing ferromagnetic order into a topological insulator system without compromising its distinctive quantum coherent features could lead to the realization of several predicted physical phenomena[6,7]. In particular, achieving robust long-range magnetic order at the surface of the topological insulator at specific locations without introducing spin-scattering centres could open up new possibilities for devices. Here we use spin-polarized neutron reflectivity experiments to demonstrate topologically enhanced interface magnetism by coupling a ferromagnetic insulator (EuS) to a topological insulator (Bi_2Se_3) in a bilayer system. This interfacial ferromagnetism persists up to room temperature, even though the ferromagnetic insulator is known to order ferromagnetically only at low temperatures (<17 K). The magnetism induced at the interface resulting from the large spin–orbit interaction and the spin–momentum locking of the topological insulator surface greatly enhances the magnetic ordering (Curie) temperature of this bilayer system. The ferromagnetism extends ~2 nm into the Bi_2Se_3 from the interface. Owing to the short-range nature of the ferromagnetic exchange interaction, the time-reversal symmetry is broken only near the surface of a topological insulator, while leaving its bulk states unaffected. The topological magneto-electric response originating in such an engineered topological insulator[2,8] could allow efficient manipulation of the magnetization dynamics by an electric field, providing an energy-efficient topological control mechanism for future spin-based technologies.

Realizing a ferromagnetic surface state in a topological insulator (TI) is predicted to allow several prominent phenomena to emerge, such as the interfacial magneto-electric effect[9], the electric-field-induced image magnetic monopole[1,2], and Majorana fermions[10]. To achieve this goal, we need to introduce ferromagnetism at the surface of the TI while leaving its bulk properties unchanged[11]. The magnetic proximity by interfacial exchange coupling[12] allows us to avoid the introduction of defects and reliably to separate bulk from surface state effects, which are advantages over magnetic bulk doping[13] or surface doping by magnetic adatoms[14]. In practice, the current technology of inducing magnetism in TI is confined to low temperatures. Furthermore, there is a lack of experimental evidence and of detailed understanding of the proximity-induced magnetism, restricting its potential for applications. A key requirement for useful applications is the generation of room-temperature ferromagnetism in the TI[15].

We engineered hybrid heterostructures of a TI (Bi_2Se_3) combined with a ferromagnetic insulator (FMI) (EuS) in bilayers grown with well defined atomically sharp interfaces and crystalline orientation. We elucidate the interactions at the interface between TI and FMI using depth-sensitive polarized neutron reflectometry (PNR). Using PNR we directly observe the emergence of a ferromagnetic state in the top two quintuple layers (QL, where 1 QL ≈ 0.96 nm) of Bi_2Se_3 near the TI–FMI interface. This ferromagnetic state in the TI persists up to temperatures larger than 300 K, far above the Curie temperature (above which the material normally loses its magnetism) of ~17 K of bulk EuS. The observation of an anomalous Hall effect provided additional evidence of a perpendicular moment in the TI that persists to high temperatures. Our findings demonstrate that such hybrid heterostructures can be implemented to achieve a robust and uniform surface magnetism in the TI, with high-quality coverage over a large area, which is a fundamental step towards device design.

We grew hybrid Bi_2Se_3–EuS bilayer structures by molecular beam epitaxy on sapphire (Al_2O_3(0001)) substrates. The X-ray diffraction (XRD) scans along the growth direction for different bilayer configurations and for a Bi_2Se_3 film alone are shown in Fig. 1a. The plots clearly show EuS(111) peaks for EuS layers 2–10 nm thick on different Bi_2Se_3 layer thicknesses. The microstructure of the layers is visible in the cross-sectional high-resolution transmission electron microscopy (TEM) images in Fig. 1b and c, showing that EuS and Bi_2Se_3 are both coherently aligned along the (111) and the (0001) directions, respectively, and an atomically sharp interface is formed at the boundary. The QL structure of Bi_2Se_3 is clearly resolved, whereas individual atomic planes are seen for EuS (in Fig. 1c). XRD and high-resolution TEM thus confirm the formation of highly ordered heterostructures for all samples. The interface quality was further confirmed with soft X-ray absorption spectroscopy, simultaneously using surface- and bulk-sensitive techniques, which indicate a sharp electronic interface between EuS and Bi_2Se_3 (see Extended Data Fig. 1 for details).

Thin films of EuS on Si substrates generally favour in-plane magnetic anisotropy even down to a 1-nm thickness[16]. However, we find that in close proximity with Bi_2Se_3, the strong spin–orbit coupling modifies the in-plane anisotropy[17,18], thereby leading to an out-of-plane magnetic moment in the TI surface state[12]. We found that all films display a remanent moment in both in-plane and out-of-plane geometries (see Extended Data Fig. 2), where the out-of-plane remanence is a clear signature of the normally in-plane moment being tilted out-of-plane. This tilting was found to increase for thinner TI films, suggesting an enhanced out-of-plane preference. To understand the nature of the anisotropy, superconducting quantum interference device (SQUID) magnetometry of different thicknesses of EuS and

[1]Department of Physics, Massachusetts Institute of Technology, Cambridge, Massachusetts 02139, USA. [2]Francis Bitter Magnet Laboratory, Massachusetts Institute of Technology, Cambridge, Massachusetts 02139, USA. [3]Plasma Science and Fusion Center, Massachusetts Institute of Technology, Cambridge, Massachusetts 02139, USA. [4]Quantum Condensed Matter Division, Neutron Sciences Directorate, Oak Ridge National Laboratory, Oak Ridge, Tennessee 37831, USA. [5]Institut fuer Theoretische Physik III, Ruhr-Universitaet Bochum, D-44801 Bochum, Germany. [6]Institute for Theoretical Solid State Physics, Institut fuer Festkoerper- und Werkstoffforschung, Dresden, D-01069 Dresden, Germany. [7]Department of Physics, Northeastern University, Boston, Massachusetts 02115, USA. [8]Département de Physique, Ecole Normale Supérieure, Centre National de la Recherche Scientifique, Paris Sciences et Lettres Research University, Paris 75005, France. [9]Saha Institute of Nuclear Physics, 1/AF Bidhannagar, Kolkata 64, India. [10]Advanced Photon Source, Argonne National Laboratory, Argonne, Illinois 60439, USA.
*These authors contributed equally to this work.

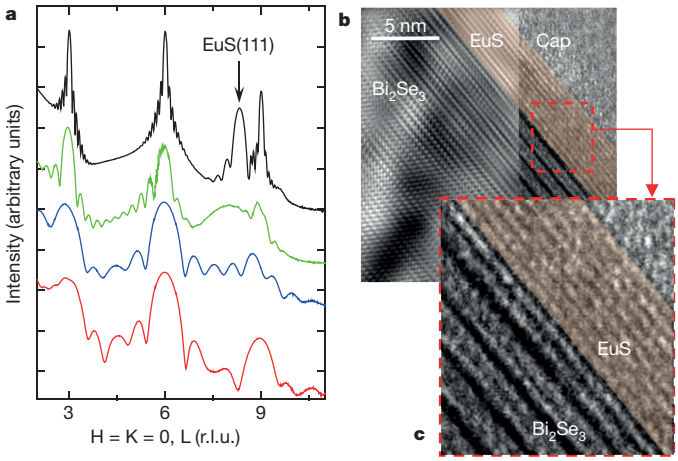

Figure 1 | XRD and high-resolution TEM of Bi_2Se_3–EuS bilayers. **a**, XRD line scans along the L-direction (growth direction) for the bilayers with different Bi_2Se_3 and EuS thicknesses show that [111]-EuS is parallel to [0001]-Bi_2Se_3. Bi_2Se_3–EuS bilayers of thickness 30 QL/10 nm (black), 10 QL/2 nm (green) and 5 QL/1 nm (blue) are shown. In addition Bi_2Se_3 (red) without EuS of thickness 5 QL is shown for comparison. Well defined Kiessig fringes are an indication of good correlation between the top surface of EuS and the interface of EuS and Bi_2Se_3. The graph is base-10 logarithmic on the *y* axis (scattered intensity) and linear on the *x* axis, where H, K, and L stand for the Miller indices in units of the reciprocal lattice (r.l.u.) of the Bi_2Se_3(0001) surface. **b**, Fourier-filtered cross-sectional high-resolution TEM image for the Bi_2Se_3–EuS interface. Bilayers are protected with an amorphous Al_2O_3 cap layer (Cap). **c**, Expanded image of the Bi_2Se_3–EuS interface, showing the defect-free and cluster-free atomically sharp bilayer interface.

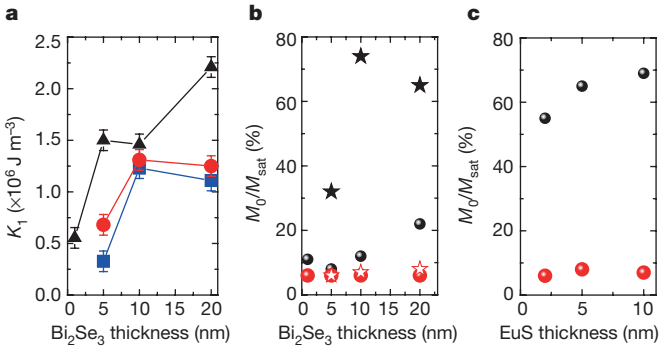

Figure 2 | SQUID magnetometry measurements for different Bi_2Se_3–EuS bilayers. **a**, Magnetic anisotropy, K_1, for various bilayer thickness combinations (the EuS thickness of 10 nm is shown in blue, 5 nm in red and 1 nm in black). The error bars come from the computation of M_{sat} from SQUID measurements. **b** and **c**, In-plane (IP, black) and out-of-plane (OP, red) remanence ratios M_0/M_{sat} for different bilayer samples are extracted from $M(H)$ loops for each sample. **b**, The EuS thickness is fixed at 1 nm (samples shown as circle symbols) and 5 nm (samples shown as star symbols) and Bi_2Se_3 ranges from 1 QL up to 20 QL. **c**, The Bi_2Se_3 thickness (20 QL) is fixed and EuS thicknesses range from 2 to 10 nm.

Bi_2Se_3 bilayer combinations were compared. To quantify this change in magnetic anisotropy as a function of bilayer parameters we measured the in-plane anisotropy constant $K_1 = \frac{1}{2}\mu_0 H_A M_{sat}$ (ref. 19) and the remanence ratio M_0/M_{sat}. Here, M_0 is the magnetization at zero applied field, M_{sat} is the saturation magnetization, and H_A is the saturation field in the out-of-plane direction. Figure 2 plots K_1 and M_0/M_{sat} for various Bi_2Se_3 and EuS thicknesses. Interestingly, the in-plane anisotropy constant decreases systematically as the thickness of Bi_2Se_3 is reduced (Fig. 2a). This is accompanied by a decrease in the remanence ratio in the in-plane direction as expected (Fig. 2b). The same decrease in the remanence ratio is observed when the EuS thickness is decreased (Fig. 2c). In contrast, we found that the out-of-plane remanence ratio is remarkably unaffected when either thickness is changed, suggesting that the out-of-plane component is an interface effect. We measured an average remanence of ~6% in the out-of-plane direction.

From the magnetization studies above and also from a previous study[12], we expect the Bi_2Se_3 layer to become magnetic and spin-polarized owing to the exchange coupling with the adjacent FMI layer. The experimentally observed out-of-plane component is necessary for splitting the bands in the TI and breaking the time-reversal symmetry at the interfacial region adjacent to the FMI[1,2,8,20]. This can be regarded as a consequence of the strong spin–orbit coupling, which leads to the locking of spin to momentum, with the in-plane fluctuations contributing to the Berry phase[21–23].

To understand the exchange interaction better and to explore the depth profile of the magnetism at the interface directly, we used a depth-sensitive PNR technique[24]. The depth profiles of the nuclear and magnetic scattering length densities (NSLD and MSLD; see Extended Data Fig. 3 for details) correspond to the depth profile of the chemical and in-plane magnetization vector distributions, respectively. PNR measurements were carried out on the bilayers with EuS thickness fixed at 5 nm and Bi_2Se_3 thickness varied (5 QL, 10 QL and 20 QL). Figure 3b shows results of R^+ and R^- reflectivity, where the superscript plus (or minus) signs indicate neutrons with spin parallel (or antiparallel) to the direction of the applied magnetic field, for samples measured at 5 K with the in-plane magnetic field $H_{ext} = 1$ T after the samples were cooled at zero magnetic field. The NSLD and MSLD depth profiles were obtained from a simultaneous fit to the data and plotted as functions of the depth from the surface and shown in Fig. 3c for the sample with 20 QL Bi_2Se_3 (see Extended Data Fig. 3 for samples with 5 QL and 10 QL). PNR reveals a sharp interface between the EuS and Bi_2Se_3 layers over the whole lateral size of the sample with average roughness ~0.2 nm, as also observed by cross-sectional TEM. The absorption scattering length density (ASLD) depth profile (Fig. 3c), which is the signature of solely Eu atoms, stops at a certain depth, demonstrating that no Eu atoms are detected in the Bi_2Se_3 layer.

Remarkably, the magnetization profile MSLD shows a magnetization of 240 electromagnetic units (emu) cm^{-3} and 34 emu cm^{-3} in the first and second QL of Bi_2Se_3, respectively (marked with red arrows in Fig. 3c, where the Eu absorption length is shown as a blue curve), penetrating into Bi_2Se_3 beyond the EuS–Bi_2Se_3 interface. There is a concurrent reduction in the EuS magnetization observed near the interface, where 1.5 nm of the EuS layer has the moment reduced to 2.5 Bohr magnetons (μ_B) per Eu^{2+} (blue arrow in Fig. 3c), which is only about ~36% of the maximum 7μ_B per Eu^{2+} in the bulk of the EuS. Given that the NSLD depth profile of the EuS layer is uniform and no changes are detected in the structural and chemical composition in this interfacial EuS layer, we attribute the reduced in-plane magnetization in this thin interfacial EuS layer to a canting of the Eu magnetization vector towards the out-of-plane direction. Since the out-of-plane component of the magnetization vector is parallel to the momentum transfer *Q*, it is thus not responsive in PNR[25]. This is consistent with the observation of the out-of-plane magnetization component in SQUID measurements (Fig. 2). The sample's reflectivity below its critical edge, called the total reflection region, is unity if there is no absorption[26]. The inset of Fig. 3b shows a magnified region of the total reflection. Here, the impact of the Eu absorption cross-section on the PNR reflectivity results in a striking feature in the total reflection region of R^+ and R^-, which is very sensitive to the depth profile of the Eu atoms. The ASLD profile in Fig. 3c shows a sharp interface between the EuS and Bi_2Se_3 layers as well, and confirms that Eu atoms are not present in the Bi_2Se_3 layer.

We investigated the magnetization behaviour of bilayers with PNR experiments above the Curie temperature (T_C) of EuS. We discovered that the heterostructures exhibit ferromagnetic behaviour even at 300 K. Figure 4a displays the spin-asymmetry (SA) ratio for the 10 QL Bi_2Se_3 sample measured at 50 K, 75 K, 120 K and 300 K. This striking observation of room-temperature ferromagnetism demonstrates that the non-zero magnetization present in the 2 QL Bi_2Se_3 interfacial layer also penetrates into the EuS layer (Fig. 4b), thus stabilizing

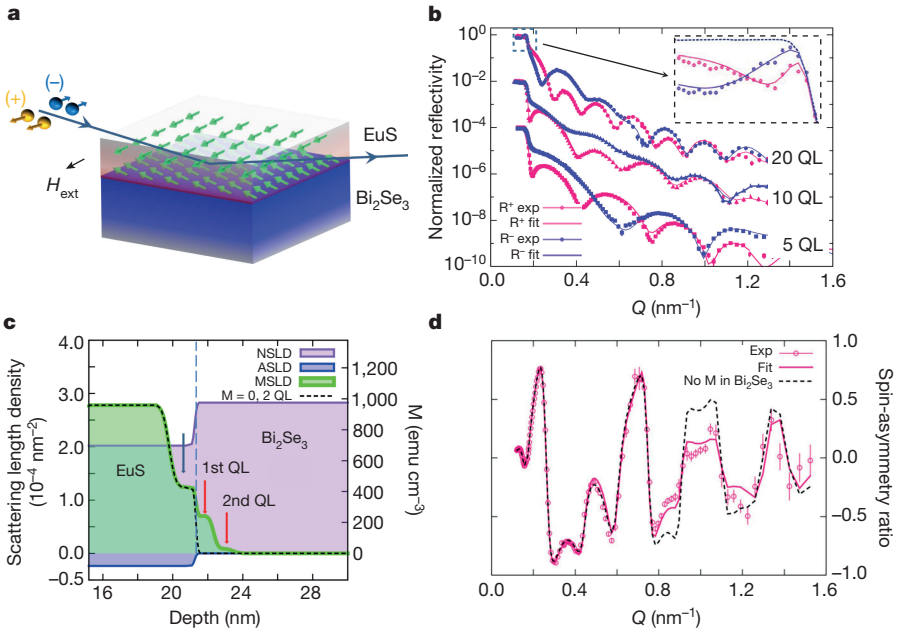

Figure 3 | Polarized neutron reflectivity results for different Bi_2Se_3–EuS bilayers. a, Schematic of the PNR experimental set-up for Bi_2Se_3–EuS bilayer films. **b**, Measured (symbols) and fitted (solid lines) reflectivity curves for spin-up (R^+) and spin-down (R^-) neutron spin-states (logarithmic–linear scale) shown as a function of momentum transfer $Q = 4\pi\sin(\theta)/\lambda$, where θ is the incident angle and λ is the neutron wavelength. The inset is an expanded view of the reflectivity below its critical edge, where the reflectivity is sensitive to the distribution of the Eu atoms owing to their absorption cross-section and their magnetic moment. The error bars represent one standard deviation. **c**, PNR nuclear (NSLD, in pink), magnetic (MSLD, in green) and absorption (ASLD, in blue) scattering length density profiles, measured for the 20 QL sample at 5 K with an external in-plane magnetic field of 1 T and presented as a function of the distance from the sample surface. The magnetization measured inside the Bi_2Se_3 layer is marked with red arrows, and the reduction of the in-plane component of EuS at the interface caused by a canting of the Eu magnetization vector towards the OP direction is marked with a blue arrow. The scale on the right-hand-side shows magnetization M. **d**, PNR spin-asymmetry (SA) ratio $SA = (R^+ - R^-)/(R^+ + R^-)$ obtained from the experimental and fitted reflectivities in **b**. The fit with zero magnetization ($M = 0$ in 2 QL) in the Bi_2Se_3 layer (black dashed line in **d** obtained with the corresponding MSLD profile also shown with black dashed line in **c**) has a large deviation from the experimental data. The error bars represent one standard deviation.

the magnetization well above its T_C. The magnitude of the Bi_2Se_3 moment as a function of temperature is shown in Fig. 4c: although the TI moment is reduced by an order of magnitude at 120 K compared to its 5 K value, and by another factor of two or more at room temperature, it remains nevertheless substantial. No magnetization was detected above ~50 K in the pure EuS film when measured under the same experimental conditions as in bilayer films (see Extended Data Fig. 3 for details).

Thus we have successfully established ferromagnetic order at the surface of epitaxial Bi_2Se_3 films using internal exchange coupling through proximity with the ferromagnetic insulator EuS. PNR provides direct evidence that Bi_2Se_3–EuS heterostructures exhibit proximity-induced interfacial magnetization in the top 2 QL (~2 nm) layer of Bi_2Se_3. Thus PNR enables us efficiently to distinguish the magnetic TI surface states from the trivial bulk states. We show that such effects originate through exchange interaction, without structural perturbation at the interface. Our PNR, magnetization, and transport studies reveal that magnetic moment persists in the TI at temperatures far above the Curie temperature of the FMI, signifying a robust topological magnetic state of the bilayer system. Owing to the short-range nature of this ferromagnetic exchange interaction, we are able to locally break the time-reversal symmetry on the surface of the TI while leaving its bulk states unaffected. Finally, the results reported here pave the way for a new class of spin-based electronics driven by gapped Dirac surface states. For instance, high-temperature ferromagnetism in gated FMI–TI–FMI structures may allow for the stabilization and

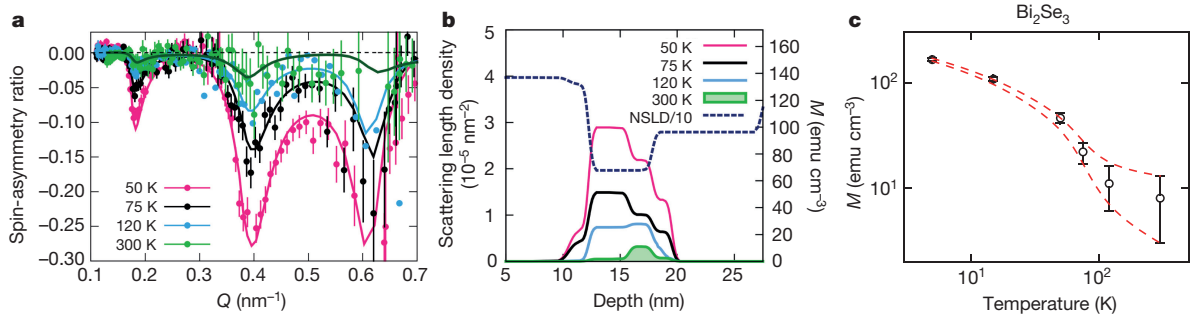

Figure 4 | Ferromagnetic order in Bi_2Se_3–EuS bilayer samples. a, PNR measurements of a Bi_2Se_3 10 QL EuS bilayer film. The measured SA at different temperatures and model fits (shown with solid lines), where the sample was cooled at zero magnetic field then measured at 50 K, 75 K, 120 K and 300 K while warming. The error bars represent one standard deviation. **b**, Chemical (NSLD, dashed line) and magnetic (MSLD) depth profiles at different temperatures (solid lines for temperatures 50 K, 75 K and 120 K and green shading for 300 K) are presented as a function of the distance from the sample surface. The scale on the right-hand side shows magnetization M. **c**, PNR-derived magnetization of Bi_2Se_3 as a function of temperature (logarithmic–logarithmic scale). The error bars indicate the confidence interval.

observation of the topological magnetoelectric effect. This would lead to unprecedented control of spin and charge carriers by means of a topological magnetoelectric bias mechanism.

Online Content Methods, along with any additional Extended Data display items and Source Data, are available in the online version of the paper; references unique to these sections appear only in the online paper.

Received 9 April 2015; accepted 3 March 2016.
Published online 9 May 2016.

1. Hasan, M. Z. & Kane, C. L. Colloquium: Topological insulators. *Rev. Mod. Phys.* **82,** 3045–3067 (2010).
2. Qi, X.-L. & Zhang, S.-C. Topological insulators and superconductors. *Rev. Mod. Phys.* **83,** 1057–1110 (2011).
3. Fu, L. & Kane, C. L. Superconducting proximity effect and Majorana fermions at the surface of a topological insulator. *Phys. Rev. Lett.* **100,** 096407 (2008).
4. Akhmerov, A., Nilsson, J. & Beenakker, C. Electrically detected interferometry of Majorana fermions in a topological insulator. *Phys. Rev. Lett.* **102,** 216404 (2009).
5. Ferreira, G. J. & Loss, D. Magnetically defined qubits on 3D topological insulators. *Phys. Rev. Lett.* **111,** 106802 (2013).
6. Chang, C. Z. *et al.* Experimental observation of the quantum anomalous Hall effect in a magnetic topological insulator. *Science* **340,** 167–170 (2013).
7. Checkelsky, J. G. *et al.* Trajectory of the anomalous Hall effect towards the quantized state in a ferromagnetic topological insulator. *Nature Phys.* **10,** 731–736 (2014).
8. Qi, X.-L., Hughes, T. L. & Zhang, S.-C. Topological field theory of time-reversal invariant insulators. *Phys. Rev. B* **78,** 195424 (2008); erratum *Phys. Rev. B* **81,** 159901 (2010).
9. Essin, A., Moore, J. & Vanderbilt, D. Magnetoelectric polarizability and axion electrodynamics in crystalline insulators. *Phys. Rev. Lett.* **102,** 146805 (2009); erratum *Phys. Rev. Lett.* **103,** 259902 (2009).
10. Nadj-Perge, S. *et al.* Observation of Majorona fermions in ferromagnetic atomic chains on a superconductor. *Science* **346,** 602–607 (2014).
11. Scholz, M. R. *et al.* Tolerance of topological surface states towards magnetic moments: Fe on Bi_2Se_3. *Phys. Rev. Lett.* **108,** 256810 (2012).
12. Wei, P. *et al.* Exchange-coupling-induced symmetry breaking in topological insulators. *Phys. Rev. Lett.* **110,** 186807 (2013).
13. Chen, Y. L. *et al.* Massive Dirac fermion on the surface of a magnetically doped topological insulator. *Science* **329,** 659–662 (2010).
14. Vobornik, I. *et al.* Magnetic proximity effect as a pathway to spintronic applications of topological insulators. *Nano Lett.* **11,** 4079–4082 (2011).
15. Mellnik, A. R. *et al.* Spin-transfer torque generated by a topological insulator. *Nature* **511,** 449–451 (2014).
16. Miao, G.-X. & Moodera, J. S. Controlling magnetic switching properties of EuS for constructing double spin filter magnetic tunnel junctions. *Appl. Phys. Lett.* **94,** 182504 (2009).
17. Chappert, C. & Bruno, P. Magnetic anisotropy in metallic ultrathin films and related experiments on cobalt films. *J. Appl. Phys.* **64,** 5736 (1988).
18. Semenov, Y. G., Duan, X. & Kim, K. W. Electrically controlled magnetization in ferromagnet-topological insulator heterostructures. *Phys. Rev. B* **86,** 161406 (2012).
19. Stoehr, J. & Siegmann, H. C. *Magnetism: From Fundamentals to Nanoscale Dynamics* (Springer, 2006).
20. Xu, S.-Y. *et al.* Hedgehog spin texture and Berry's phase tuning in a magnetic topological insulator. *Nature Phys.* **8,** 616–622 (2012).
21. Yokoyama, T., Zang, J. & Nagaosa, N. Theoretical study of the dynamics of magnetization on the topological surface. *Phys. Rev. B* **81,** 241410 (2010).
22. Tserkovnyak, Y. & Loss, D. Thin-film magnetization dynamics on the surface of a topological insulator. *Phys. Rev. Lett.* **108,** 187201 (2012).
23. Nogueira, F. S. & Eremin, I. Fluctuation-induced magnetization dynamics and criticality at the interface of a topological insulator with a magnetically ordered layer. *Phys. Rev. Lett.* **109,** 237203 (2012).
24. Lauter, V., Ambaye, H., Goyette, R., Hal Lee, W.-T. & Parizzi, A. Highlights from the magnetism reflectometer at the SNS. *Physica B* **404,** 2543–2546 (2009).
25. Zhu, T. *et al.* The study of perpendicular magnetic anisotropy in CoFeB sandwiched by MgO and tantalum layers using polarized neutron reflectometry. *Appl. Phys. Lett.* **100,** 202406 (2012).
26. Korneev, D. A. *et al.* Absorbing sublayers and their influence on the polarizing efficiency of magnetic neutron mirrors. *Nucl. Instrum. Meth. Phys. Res. B* **63,** 328–332 (1992).

Acknowledgements F.K. thanks L. Fu, V. Madhavan, N. Gedik, B. Sinkovic, Y. Wang and H. Lin for discussions. V.L. thanks S. Nagler for discussions, and H. Ambaye, A. Glavic and the Spallation Neutron Source staff for support. The research conducted at ORNL's Spallation Neutron Source was sponsored by the Scientific User Facilities Division, Office of Basic Energy Sciences, and the US Department of Energy. F.K., P.J.-H., and J.S.M. thank the MIT MRSEC through the MRSEC Program of the National Science Foundation under award number DMR-0819762 (upgrade of the molecular beam epitaxy system) for support. J.S.M. thanks the National Science Foundation (DMR-1207469), Office of Naval Research (N00014-13-1-0301) and the STC Center for Integrated Quantum Materials under National Science Foundation grant DMR-1231319 for support, and the thin-film growth and characterization of the materials used. The hetero-structure characterization was supported by the US Department of Energy, Basic Energy Sciences Office, Division of Material Sciences and Engineering under award number DE-SC0006418 (F.K. and P.J.-H.). B.A.A., M.E.J. and D.H. thank the National Science Foundation under award numbers DMR-0907007 and ECCS-1402738 (for SQUID magnetometry characterization) for support. B.A.A. is also supported in part by the Agence Nationale de la Recherche LabEx grants ENS-ICFP (ANR-10-LABX-0010/ ANR-10-IDEX-0001-02 PSL). The use of the Advanced Photon Source was supported by the US Department of Energy, Office of Science, Office of Basic Energy Sciences, under contract number DE-AC02-06CH11357. I.E. and F.S.N. acknowledge the German Research Council (DFG) for the financial support under the collaborative research centre SFB TR 12 and the priority programme SPP 1666 (grant number ER 463/9).

Author Contributions The research was conceived and designed by F.K. and J.S.M. The samples were prepared and characterized by F.K. The XRD experiments and data analysis were carried out by F.K.; the high-resolution TEM experiments and data analysis were carried out by B.S.; the PNR experiments and data analysis were carried out by V.L.; the XAS/XMCD experiments and data analysis were carried out by F.K. and J.W.F.; the transport experiments and data analysis were carried out by F.K. and D.H.; and the SQUID experiments and data analysis were carried out by F.K., B.A.A., M.E.J. and D.H. The data was interpreted by F.K., V.L., F.S.N. and J.S.M. All authors discussed the results and commented on the manuscript. The manuscript was written by F.K., V.L. and F.S.N.

Author Information Reprints and permissions information is available at www.nature.com/reprints. The authors declare no competing financial interests. Readers are welcome to comment on the online version of the paper. Correspondence and requests for materials should be addressed to F.K. (katmis@mit.edu) or J.S.M. (moodera@mit.edu).

METHODS

Material growth. The growth of Bi_2Se_3–EuS bilayer systems were carried out in a molecular beam epitaxy apparatus under an ultrahigh-vacuum environment (10^{-9}–10^{-10} Torr). High-purity (5 N) Bi and Se constituents were thermally co-evaporated from separate Knudsen cells adjusted to obtain a 2:3 Bi:Se deposition ratio as determined by an *in situ* crystal monitor during growth and confirmed by *ex situ* X-ray reflectivity measurements. (0001)-oriented Al_2O_3 wafers were used as a substrate. To improve the surface quality of the substrates *ex situ* chemical cleaning and *in situ* thermal plus oxygen plasma treatments were performed. After surface preparation, the substrate temperature was kept to 240 ± 5 °C to obtain relatively large surface mobility for epitaxial crystalline Bi_2Se_3 growth. Owing to the high reactivity of Eu atoms and the dissociation problems of S, the EuS was evaporated congruently from a single electron-beam source onto the Bi_2Se_3 layer at a rate of 0.5–0.6 Å s^{-1} without breaking the ultrahigh-vacuum condition. All devices were protected by covering the bilayers with an amorphous Al_2O_3 cap layer via *in situ* electron beam evaporation at room temperature immediately after EuS deposition, without breaking the ultrahigh vacuum.

Interface formation. The interface between EuS and Bi_2Se_3 is analysed using *in situ* reflection high-energy electron diffraction (RHEED). Extended Data Fig. 4a shows a two-dimensional-like (2D-like) (streaky) surface, which is an indication of an atomically flat Bi_2Se_3 surface. EuS is grown at room temperature, which is not enough to give sufficient surface mobility to EuS molecules. Therefore, above a certain critical thickness, which is about 3–4 nm, surface roughening occurs. The RHEED image shows the streaky feature (2D-dominant) for 2-nm-thick EuS grown on Bi_2Se_3, which we can also call the quasi-2D (2D + 3D) growth mode (Extended Data Fig. 4b and c). After deposition of 5-nm-thick EuS, RHEED images transform from the 2D-dominant to the 3D-dominant phase, which is an indication of a surface roughening (Extended Data Fig. 4d).

X-ray diffraction measurements. A well collimated nearly background-free beam is impinged on the sample surface and X-ray scattering intensity was collected by a two-dimensional charged-coupled device (CCD). The incoming beam is diffracted by a Ge (220) 4-bounce crystal monochromator to obtain CuKα1 radiation (wavelength $\lambda = 1.54056$ Å). Because of the higher intensity of the Bragg spots, the sample alignments are done on Bi_2Se_3 layer reflections instead of stronger substrate reflections and scans are performed along the Bi_2Se_3 L-rod (growth direction). The Bragg reflections are indexed according to the Bi_2Se_3 bulk hexagonal unit cell. The x-axis in Fig. 1 is indexed in terms of the hexagonal unit cell of the Bi_2Se_3, as indicated by $H = K = 0$ with different L, where $L = 3, 6, 9, \ldots$ are allowed reflections ((0003), (0006), (0009),…), where H, K, and L are the Miller indices. The Bragg reflection for EuS is calculated by the scattering angles of the peaks and fitted to the bulk EuS unit cell.

TEM. The morphology and structural properties of the layers were separately investigated by scanning TEM and high-resolution TEM. The cross-sectional TEM specimens were prepared using conventional mechanical grinding and dimpling down to below 20 μm followed by low-energy (2 keV) and low-angle (4°) Ar-ion milling. TEM images were acquired using a FEI, Tecnai G^2 F30, S-Twin microscope operating at 300 kV equipped with a Gatan Orius CCD camera.

SQUID magnetometry measurements. The ferromagnetic properties of the Bi_2Se_3–EuS bilayers were determined by magnetization measurements performed in a Quantum Design SQUID magnetometer. Both in-plane and out-of-plane magnetic properties were measured in the temperature range 2–400 K and applied magnetic fields up to 5 T (Extended Data Fig. 2).

It is known that any distortion reducing the lattice spacing of EuS increases the exchange interaction, thereby increasing both T_C and the spin stiffness[27]. Our EuS films grown on Bi_2Se_3 have shown compressive stress caused by a ~2%–10% (depends on the bilayer configuration) lattice mismatch, leading to a reduced lattice spacing. Given the large carrier density of the TI surface present at the TI–FMI interface, this is a possible phenomenon that could enhance the Curie temperature of EuS at the interfacial region. Past studies have shown that the electron doping of Eu chalcogenides can enhance the Curie temperature of the material owing to the increased indirect exchange interaction among Eu^{2+} neighbouring ions[27–30]. In a recent work, 2% Gd doping was also shown to be effective in increasing the Curie temperature of EuS up to 86.3 K (ref. 31).

The experimental results reported in the main text indicate an extraordinary upwards shift at the interface relative to the bulk value of the Curie temperature in EuS. Typically, all known examples have $\Delta T_C < 1$, whereas the results reported here indicate a shift considerably larger than unity. One example of a large upwards shift in the Curie temperature is provided by $Ni_3Fe(111)$, which has a bulk Curie temperature of 850 K, with a surface Curie temperature of 1050 K (ref. 32). The other typical example is the well known Gd(0001) surface, where the bulk and surface Curie temperature values have 293 K and 315 K, respectively[33].

PNR. PNR experiments were performed on the Magnetism Reflectometer at the Spallation Neutron Source at Oak Ridge National Laboratory. Neutrons with wavelengths within a band of 2–8 Å and with a high polarization of 99% to 98.5% were used. Measurements were performed in a closed cycle refrigerator (Advanced Research System CCR) with an applied external magnetic field by using a Bruker electromagnet with a maximum magnetic field of 1.15 T. Using the time-of-flight method[24], a collimated polychromatic beam of polarized neutrons with the wavelength band $\Delta\lambda$ impinges on the film at a grazing incidence angle θ, where it interacts with atomic nuclei and the spins of unpaired electrons (see Fig. 3a). The reflected intensity is measured as a function of momentum transfer, $Q = 4\pi\sin(\theta)/\lambda$, for two neutron polarizations R^+ and R^-, with the neutron spin parallel (+) or antiparallel (−) to the direction of the external field, H_{ext}. To separate the nuclear from the magnetic scattering, the data is presented as the spin-asymmetry (SA) ratio $SA = (R^+(Q) - R^-(Q))/(R^+(Q) + R^-(Q))$ as depicted in Fig. 3d. A value of $SA = 0$ designates no magnetic moment in the system. Being electrically neutral, spin-polarized neutrons penetrate the entire multilayer structures and probe magnetic and structural composition of the film through the buried interfaces down to the substrate. To show the sensitivity of PNR to the interfacial magnetization measured in 2 QL of Bi_2Se_3, we intentionally set the magnetization in Bi_2Se_3 to zero (dashed line in the magnetization profile in Fig. 3c) and performed calculations of the corresponding SA (dashed line in Fig. 3d), which shows a considerable deviation from the experimental data in Fig. 3d. PNR results for samples with 10 QL and 5 QL showed similar interfacial magnetization behaviour in Bi_2Se_3 (Extended Data Fig. 3).

To verify the magnetization observed at higher temperatures in the TI–FMI bilayer system, we performed additional measurements with a reference sample of pure EuS film grown on a sapphire substrate under similar conditions. Following the same experimental protocol as for the Bi_2Se_3–EuS bilayer, the EuS film was cooled at zero magnetic field to 5 K and measured in an external magnetic field of 1 T at different temperature between 5 K and 300 K. Extended Data Fig. 3e represents PNR reflectivity data measured on the EuS film at 5 K, 50 K, 80 K, 120 k, 250 K and 300 K. The data show no difference between R^+ and R^- above 50 K, that is, no magnetization is detected in the pure EuS film above 50 K. In addition, in Extended Data Fig. 3f the experimental data are presented as the SA obtained from the measured reflectivities in Extended Data Fig. 3e. The difference between R^+ and R^- normalized to their sum is very sensitive to small M values and serves to emphasize even very small M.

XAS and XMCD. X-ray absorption spectroscopy (XAS) and X-ray magnetic circular dichroism (XMCD) were used to confirm the quality of samples. We performed a series of soft X-ray absorption spectroscopy experiments at beamline 4-ID-C of the Advanced Photon Source by simultaneous measurement of the surface sensitive total electron yield and the bulk sensitive fluorescence yield. First we examine the nature of the magnetic state of the EuS layer. As shown in Extended Data Fig. 1a, the EuS layer is in a valence state of 2+ (ref. 34) and displays a large XMCD whose lineshape is consistent with a local moment of 7 μ_B per atom[35].

To examine the Bi_2Se_3 electronic structure, we measured the Se L_3 edge to probe the electronic structure of the Se. In Extended Data Fig. 1b and c, we compare the bulk-sensitive to the surface/interface-sensitive modes of XAS. For both the Al_2O_3/Bi_2Se_3 (in Extended Data Fig. 1b) and EuS/Bi_2Se_3 (in Extended Data Fig. 1c) interfaces, the agreement with the bulk is very good, indicating a bulk-like electronic structure on the surface of Bi_2Se_3. We note that the topological states occur at an energy scale below the resolution of XAS. This data, indicating a sharp electronic interface, agrees well with the diffraction and TEM data, which show the sharp interfacial structure of the bilayer.

Transport measurements. The SQUID magnetometer was also equipped with an electrical probe and used for magnetotransport measurements[36]. To probe the perpendicular magnetization of the Bi_2Se_3/EuS interface, bilayer samples were prepared for transport measurements in a Hall bar geometry by mechanically removing areas of the film. Samples were cooled down to 2–5 K in an applied perpendicular field and trained by sweeping the field between ±5 T. While warming up the samples a 4-T field was applied. Given the small signal, each Hall voltage measurement was averaged ten times at a given field value. Extended Data Fig. 5 displays results from such measurements—the saturating component of the Hall voltage (ΔV_{yx}) for two bilayer samples, 5 QL Bi_2Se_3/5 nm EuS (Extended Data Fig. 5a–d) and 7 QL Bi_2Se_3/5 nm EuS (Extended Data Fig. 5e and f), were obtained after subtracting the linear Hall component. Similar trends were observed for the two different samples, showing consistency in the behaviour of the high-temperature ferromagnetic phenomenon. However, it should be mentioned that in Bi_2Se_3 thin films the carrier density is very high (~10^{18}–10^{19} cm^{-3}), making the bulk contribution to the overall behaviour dominant, especially at higher temperatures where the surface-related effects become masked. (The mobility of the samples increased with film thickness: for example, for 5 QL the mobility was 640 $cm^2 V^{-1} s^{-1}$, whereas for 20 QL it was 1,650 $cm^2 V^{-1} s^{-1}$). Hence, precisely

measuring the surface magnetic behaviour by transport is quite challenging, as seen from the Hall data at higher temperatures. In spite of this, further support comes from XMCD measurements, carried out on the same samples, which showed magnetic behaviour similar to the PNR and Hall measurements, and also yielded magnetic moments comparable to those from SQUID measurements. The transport measurements certainly have the resolution to differentiate the interface ferromagnetic behaviour at low temperatures (below ~150 K), but not at high temperatures.

27. Mauger, A. & Godart, C. The magnetic, optical, and transport properties of representatives of a class of magnetic semiconductors: the europium chalcogenides. *Phys. Rep.* **141,** 51–176 (1986).
28. Miyazaki, H. *et al.* La-doped EuO: a rare earth ferromagnetic semiconductor with the highest Curie temperature. *Appl. Phys. Lett.* **96,** 232503 (2010).
29. Ott, H. *et al.* Soft x-ray magnetic circular dichroism study on Gd-doped EuO thin films. *Phys. Rev. B* **73,** 094407 (2006).
30. von Molnár, S. & Kasuya, T. Evidence of band conduction and critical scattering in dilute Eu-chalcogenide alloys. *Phys. Rev. Lett.* **21,** 1757–1761 (1968).
31. Idzuchi, H. *et al.* Critical exponents and domain structures of magnetic semiconductor EuS and Gd-doped EuS films near Curie temperature. *Appl. Phys. Expr.* **7,** 113002 (2014).
32. Mamaev, Y. A., Petrov, V. N. & Starovoitov, S. A. Critical behavior at surfaces. *Sov. Tech. Phys. Lett.* **13,** 642 (1987).
33. Weller, D., Alvarado, S., Gudat, W., Schröder, K. & Campagna, M. Observation of surface-enhanced magnetic order and magnetic surface reconstruction on Gd(0001). *Phys. Rev. Lett.* **54,** 1555–1558 (1985).
34. Kinoshita, T. *et al.* Spectroscopy studies of temperature-induced valence transition on $EuNi_2(Si_{1-x}Ge_x)_2$ around Eu 3*d*–4*f*, 4*d*–4*f* and Ni 2*p*–3*d* excitation regions. *J. Phys. Soc. Jpn.* **71,** 148–155 (2002).
35. Arenholz, E., Schmehl, A., Schlom, D. G. & van der Laan, G. Contribution of Eu 4*f* states to the magnetic anisotropy of EuO. *J. Appl. Phys.* **105,** 07E101 (2009).
36. Assaf, B. A. *et al.* Modified electrical transport probe design for standard magnetometer. *Rev. Sci. Inst.* **83,** 033904 (2012).

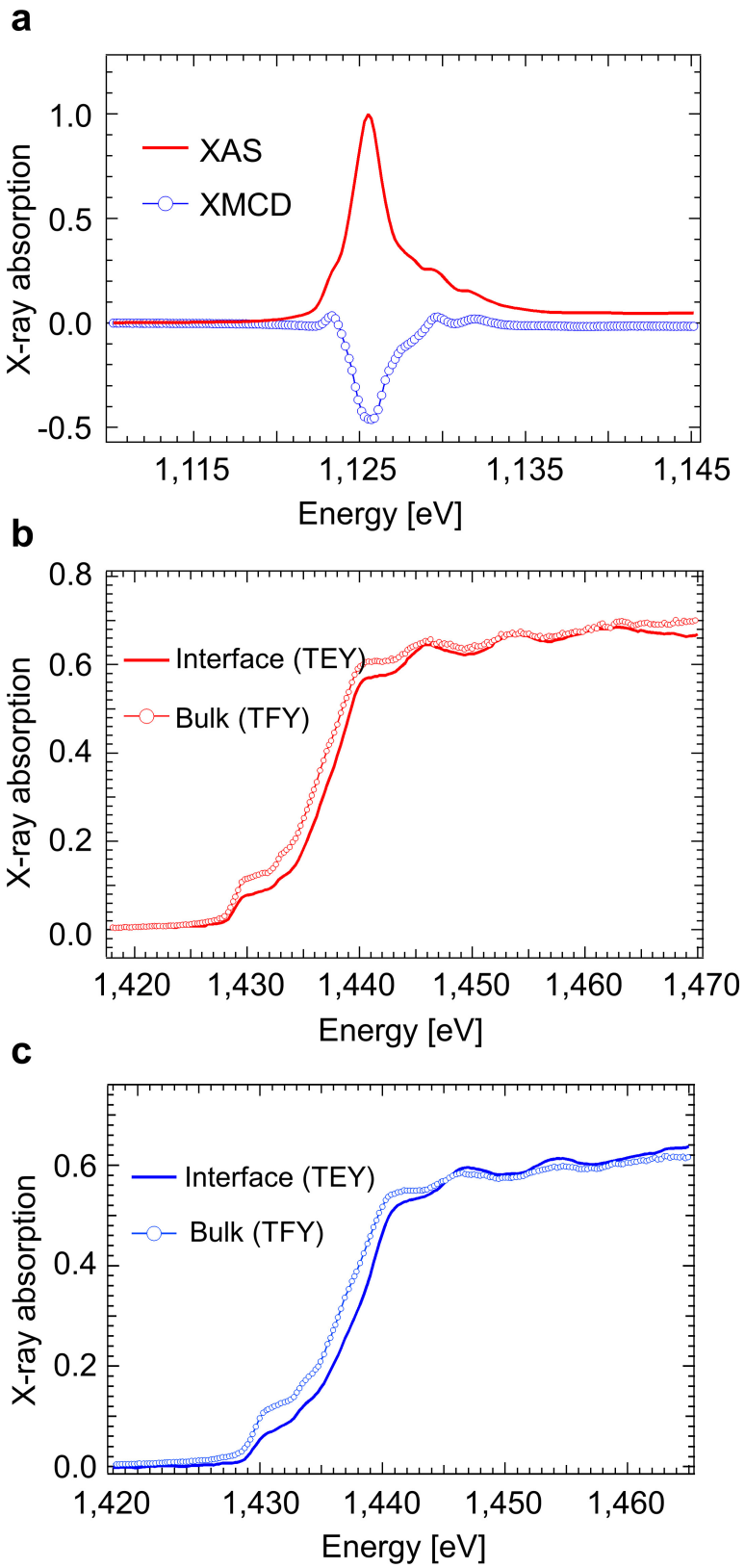

Extended Data Figure 1 | Soft X-ray absorption spectroscopy. **a**, Measurement of Eu M_5 edge at 8 K and a field of 2 T. The spectra are consistent with a valence of 2+ and the corresponding large magnetic moment seen by XMCD. **b**, **c**, X-ray absorption at the Se L edge of Al_2O_3/Bi_2Se_3 (**b**) and EuS/Bi_2Se_3 (**c**), showing the good agreement of bulk- and interface-sensitive modes, affirming that the interface and bulk have identical electronic structure. TEY, total electron yield; TFY, total fluorescence yield.

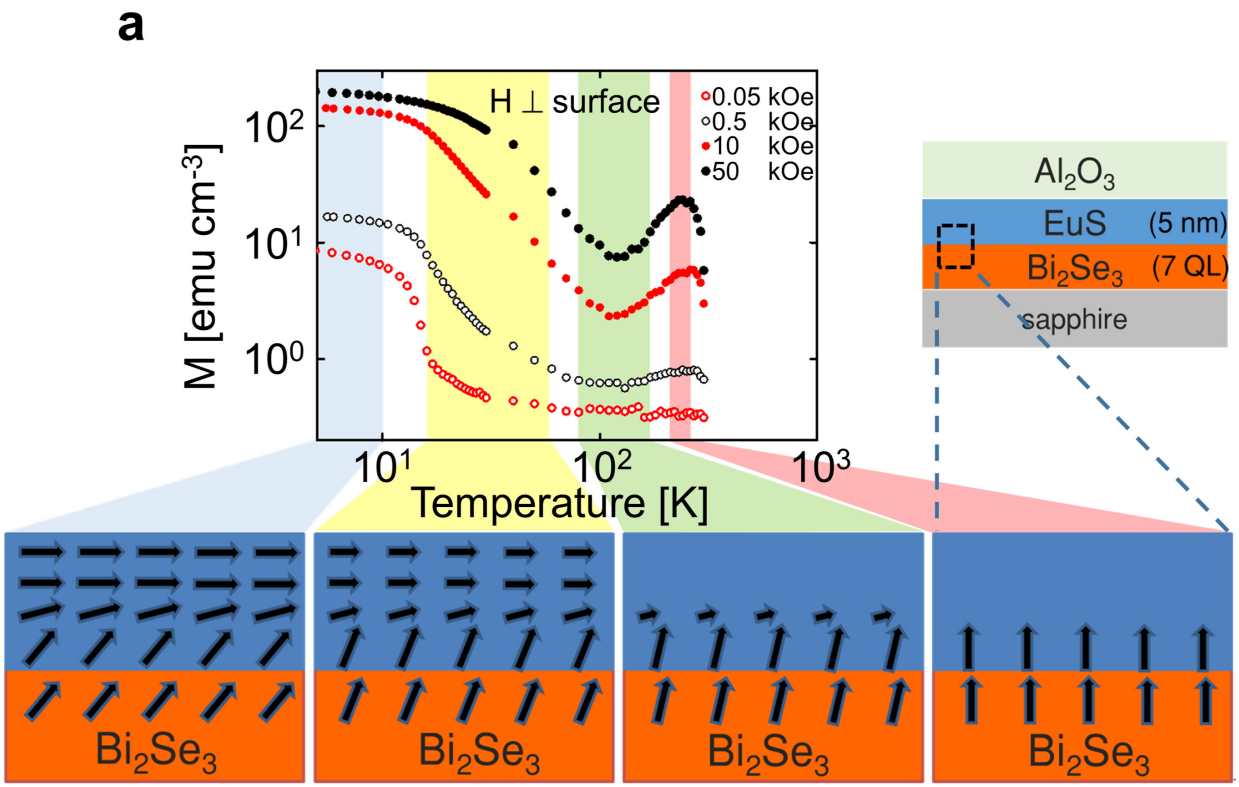

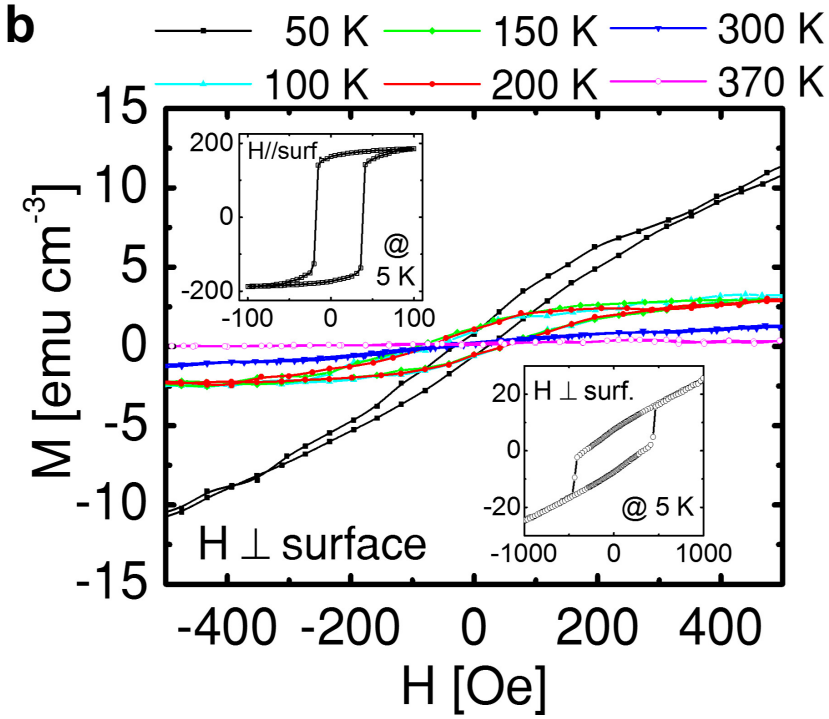

Extended Data Figure 2 | SQUID magnetometry measurements for a Bi_2Se_3–EuS bilayer with thicknesses of 7 QL for Bi_2Se_3 and 5 nm for EuS. **a**, Magnetization versus temperature at various magnetic fields applied out-of-plane (*H* perpendicular to the surface). The arrows correspond to the direction of the local magnetization. The large decrease in *M* as *T* increases shows the EuS magnetism decreasing (plotted in logarithmic–logarithmic scale). However, at higher temperatures *M*(*T*) shows an increase that is much larger than expected from Eu paramagnetism alone, and this could be attributed to reoriented spins (perpendicular) at the interface in the absence of the large in-plane influence from EuS layers above. (Furthermore, control samples of 5-nm-thick EuS grown on sapphire (Al_2O_3(0001)) substrate did not show any hysteresis above ~50 K even with a 5-T applied field). The possible spin texture is schematically represented below the experimental *M* versus *T* results. For the in-plane applied magnetic field configuration, such an increase in magnetization at high temperatures does not show features such as are observed for the perpendicular configuration. The uncertainty in *M* from the subtraction of the substrate diamagnetism is smaller than the size of the data points. **b**, The low-field magnetic hysteresis at different temperatures, where the field is applied out-of-plane (*H* perpendicular to the surface). Insets show hysteresis at 5 K comparing data for in-plane (*H* parallel to the surface) and out-of-plane magnetic-field applications.

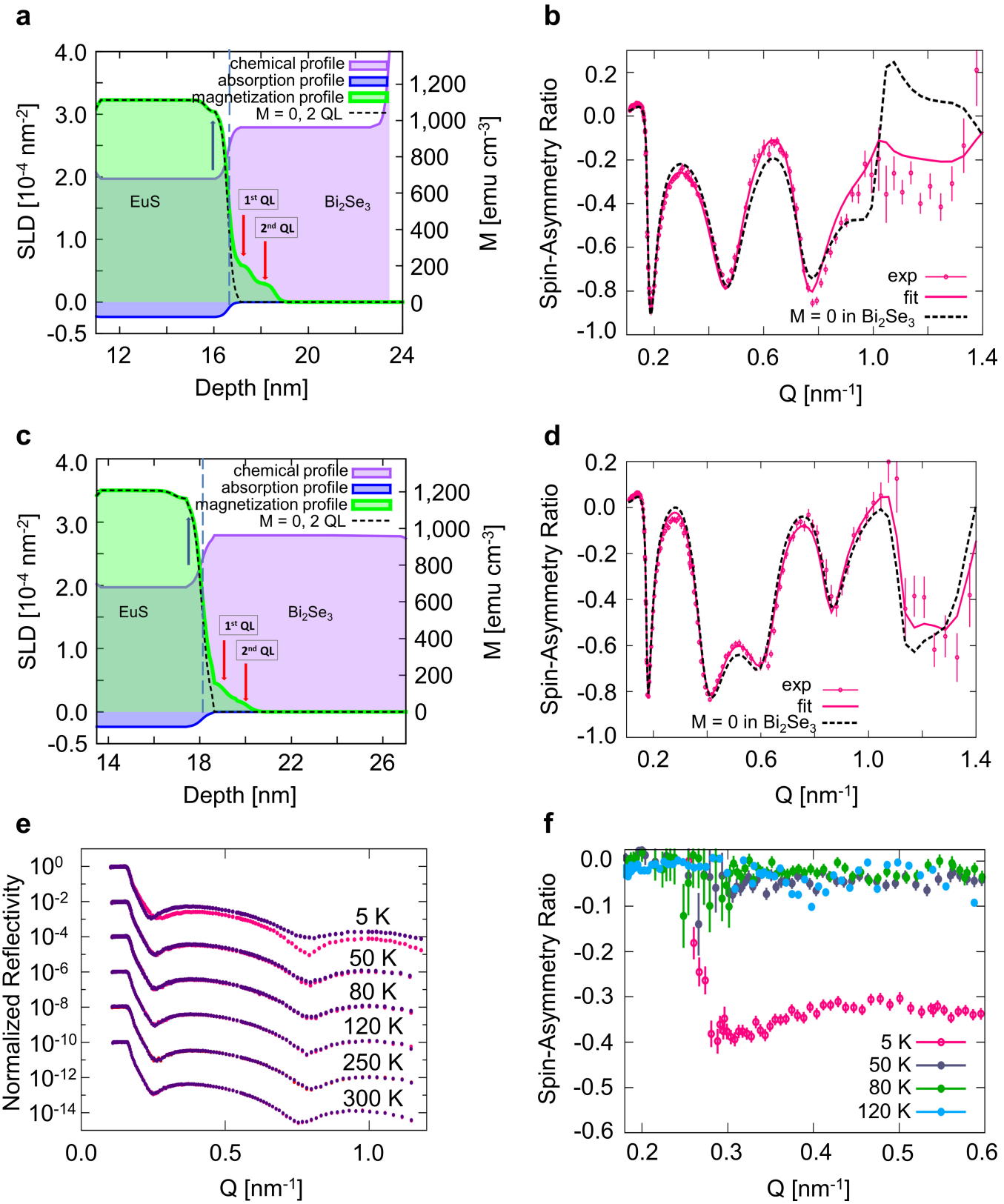

Extended Data Figure 3 | Results from PNR for Bi_2Se_3/EuS bilayer samples with 5 QL, 10 QL of Bi_2Se_3 and pure EuS. a and **c**, PNR nuclear (NSLD, in pink), magnetic (MSLD, in green) and absorption (ASLD, in blue) scattering length density (SLD) profiles, measured for samples with 5 QL (**a**) and 10 QL (**c**) at 5 K and with an in-plane magnetic field of 1 T and presented as a function of the distance from the surface. Magnetization measured inside the Bi_2Se_3 layer is marked with the red arrows. The scale on the right-hand side shows magnetization. **b** and **d**, SA as a function of the momentum transfer Q. Solid curves (dark pink) correspond to the best fits to the experimental data shown with filled circles with error bars (dark pink), with $\chi^2 = 1.32$ and 1.34, respectively; dashed curves (black) show a considerable deviation from the experimental data when the magnetization in the Bi_2Se_3 2 QL interfacial layer is set to zero with corresponding increased values of $\chi^2 = 2.82$ and 2.56. The error bars represent one standard deviation. **e**, PNR reflectivity data (logarithmic–linear scale) measured on a pure 5-nm-thick EuS film at 5 K, 50 K, 80 K, 120 K, 250 K and 300 K. **f**, Experimental data of the SA obtained from the measured reflectivities in **e**. The error bars represent one standard deviation.

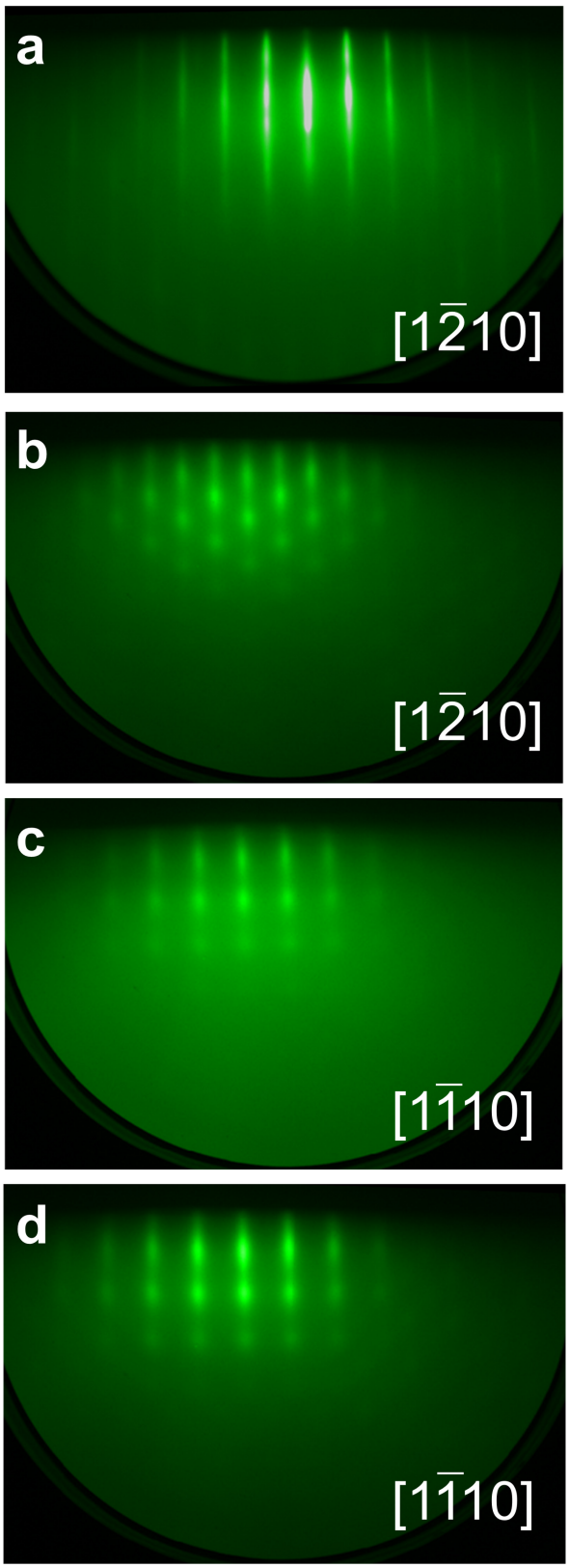

Extended Data Figure 4 | RHEED for interface evolution. a, The RHEED pattern for Bi_2Se_3 (2D-like), grown on an Al_2O_3 (0001) surface is shown, where the incident beam is along the [1$\bar{2}$10]-direction of the substrate. The RHEED pattern for the 2-nm-thick EuS surface is shown with the beam along the [1$\bar{2}$10]-direction in **b**, and along the [1$\bar{1}$10]-direction in **c**. The RHEED pattern for the 5-nm-thick EuS surface (3D-dominant) is shown along the [1$\bar{1}$10]-direction in **d**.

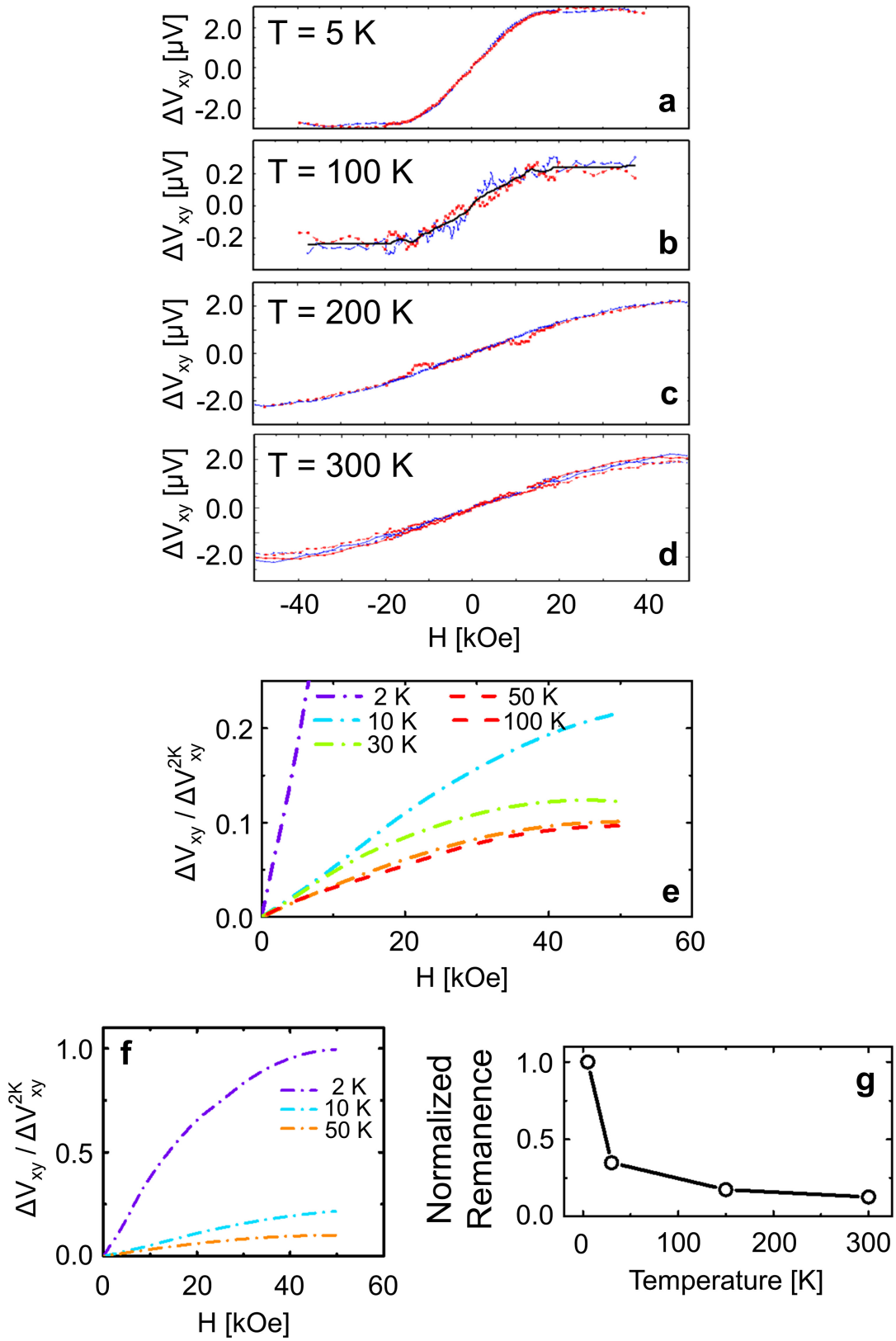

Extended Data Figure 5 | Temperature-dependent Hall voltage for a bilayer sample of 7 QL and 5 QL Bi_2Se_3 with 5-nm-thick EuS measured with 10-μA direct current, with magnetic field applied perpendicular to the film plane. A nonlinear contribution to the Hall voltage, ΔV_{yx}, is seen in the 5 QL Bi_2Se_3/5 nm EuS (**a**–**d**) and 7 QL Bi_2Se_3/5 nm EuS (**e**, **f**) samples. Plot **f** is the zoom-out of **e**. The normalized remanent magnetization in the bilayer sample (7 QL Bi_2Se_3/5 nm EuS) versus temperature (**g**), shows a finite decrease as temperature increased, matching the Hall data behaviour coming from the interfacial exchange induced ferromagnetic state, as discussed in the main text.